Received: 8 March 2021 | Revised: 29 May 2021 | Accepted: 24 June 2021

DOI: 10.1111/xen.12704

BRIEF COMMUNICATION

Xenotransplantation WILEY

Semi-automated digital quantification of cellular infiltrates for in vivo evaluation of transplanted islets of Langerhans encapsulated with bioactive materials

Matias Ramirez[1] | Guillaume Courtoy[2] | Oumaima Kharrat[1] | Michele de Beukelaer[2] | Nizar Mourad[1] | Yves Guiot[3] | Caroline Bouzin[2] | Pierre Gianello[1]

[1]Laboratory of Experimental Surgery and Transplantation, Institute of Experimental and Clinical Research, Université catholique de Louvain, Brussels, Belgium

[2]IREC Imaging Platform, Institute of Experimental and Clinical Research, Université Catholique de Louvain, Brussels, Belgium

[3]Department of Pathology, Cliniques Universitaires Saint-Luc, Brussels, Belgium

Correspondence
Matias Ramirez, UCLOUVAIN/SSS/IREC/CHEX, Avenue Hippocrate 55/B1.55.04, B-1200 Bruxelles, Belgium.
Email: matias.ramirez@uclouvain.be

Funding information
This work is supported by an EU Grant: H2020-NMP-2014-646272- BIOCAPAN

Abstract

Background: In the field of xenotransplantation, digital image analysis (DIA) is an asset to quantify heterogeneous cell infiltrates around transplanted encapsulated islets.

Materials and Methods: RGD-alginate was used to produce empty capsules or to encapsulate neonatal porcine islets (NPI) with different combinations of human pancreatic extracellular matrix (hpECM), porcine mesenchymal stem cells (pMSC) and a chitosan anti-fouling coating. Capsules were transplanted subcutaneously in rats for one month and then processed for immunohistochemistry. Immunostainings for macrophages (CD68) and lymphocytes (CD3) were quantified by DIA in two concentric regions of interest (ROI) around the capsules. DIA replicability and reproducibility were assessed by two blind operators. Repeatability was evaluated by processing the same biopsies at different time points. DIA was also compared with quantification by point counting (PC).

Results: Methodology validation: different sizes of ROIs were highly correlated. Intraclass correlation coefficients confirmed replicability and reproducibility. Repeatability showed a very strong correlation with CD3 stains and moderate/strong for CD68 stains. Group comparisons for CD68 IHC at each time point proved internal consistency. Point counting and DIA were strongly correlated with both CD3 and CD68. Capsule biocompatibility: Macrophage infiltration was higher around capsules containing biomaterials than around empty and RGD-alginate-NPI capsules. Lymphocytic infiltration was comparable among groups containing cells and higher than in empty capsules.

Conclusion: We validated a semi-automated quantification methodology to assess cellular infiltrates and successfully applied it to investigate graft biocompatibility, showing that neonatal porcine islets encapsulated in alginate alone triggered less infiltration than capsules containing islets and bioactive materials.

KEYWORDS

digital image analysis, encapsulation, islet transplantation

1 | INTRODUCTION

Encapsulated islet xenotransplantation has been proposed as a therapeutic option for Type 1 diabetes.[1-6] Encapsulation protects the graft from the immune response, thus contributing to the viability and functioning of islets.[7,8] Although less immunogenic, encapsulated cells can still lead to surrounding immune infiltrates, which needs an evaluation generally dependent on cell counting.[8-10] However, manual identification of cells encounters important limitations, such as morphological criteria (giant cells), operator dependence and errors, and is very time-consuming.

These problems could be overcome by using digital image analysis (DIA) quantification, a methodology relying on algorithms to standardize measurements of specific features on a biopsy image. The relevance of this technology has been discussed elsewhere.[11]

Here, we propose a standardized, whole slide quantification methodology to quantitatively assess immune cell infiltrates to better evaluate encapsulated islet transplants and apply this to subcutaneous grafts.

We explored bioactive encapsulation, using RGD-alginate and decellularized human pancreatic extracellular matrix (hpECM) that offer specific moieties capable of enhancing islet survival and function[12]; mesenchymal stem cells (MSCs) that have been proven beneficial when co-encapsulated with islets[10]; and an anti-fouling coating (ZW) to prevent cell adhesion and therefore hinder fibrosis.[13]

2 | MATERIALS AND METHODS

Islets were isolated as described elsewhere[14] and cultured for eight days before encapsulation to allow maturation. Biomaterials[15]and MCS[16] production are described in the Supporting Information.

2.1 | Capsule production and composition

Microcapsules (ø 500 μm) were produced using an in-house microfluidic device as described elsewhere.[17] Capsules shared shape, size and quality parameters.

Specific capsule composition of the experimental groups can be found in the Supporting Information. For the in vivo evaluation of biomaterials, where three conditions were compared, RGD-alginate was used to produce (a) empty RGD-alginate capsules (control), to encapsulate (b) neonatal porcine islets (NPI) only (basic) or (c) NPI and hpECM, pMSC and ZW (bioactive).

2.2 | In vivo evaluation

All procedures were approved by the local ethics committee [2016/UCL/MD/02]. 300g male Wistar rats were anesthetized, and two thousand capsules injected subcutaneously through an 18G needle.

After one month, implants were dissected free, fixed in formaldehyde 4% and embedded in paraffin. Following evidence from pilot studies showing a heterogeneous graft size and reaction (Figure 1), each biopsy was cut into three parts and included in separate paraffin blocks.

5 μm-thick sections underwent haematoxylin-eosin staining or immunohistochemistry (IHC). The antibodies used were as follows: for lymphocytes, rabbit anti-CD3 (Abcam, ab828) followed by anti-rabbit Envision-HRP secondary antibodies (Dako, K4003); for macrophages, mouse anti-CD68 (Abcam, ab31630) followed by donkey anti-mouse-HRP (Jackson Immunoresearch, 715-035-151). Immunostainings were revealed with DAB and nuclei counterstained with haematoxylin. The slides were then digitalized at ×20 magnification using a slide scanner (Leica® SCN400).

2.3 | Image analysis: Immunohistochemistry quantification

Each *biopsy* was divided into three *blocks*, from each of which two *images* were produced for analysis. For methodological questions, comparisons were done using blocks or images. Pooled biopsy results were used to address biological questions.

Scanned images were analysed using Visiopharm® software with house-made algorithms designed with Author®. Briefly, after

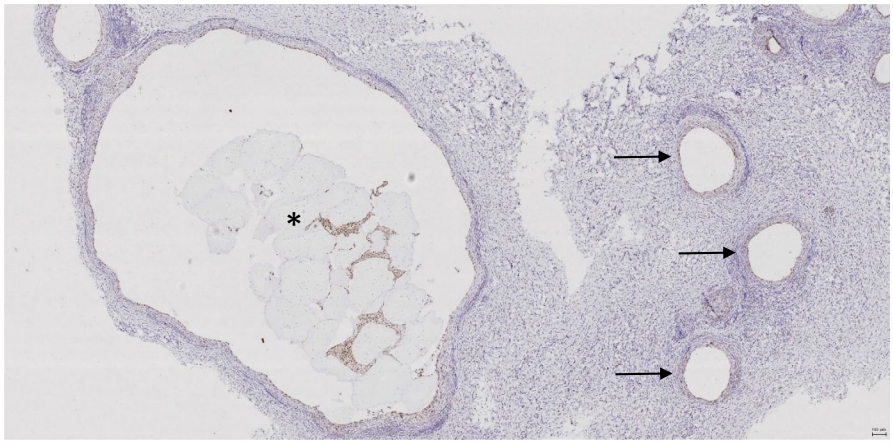

FIGURE 1 Illustration of isolated (arrows) and agglomerated (*) capsules. Scale bar: 100 μm

grafted tissue (i.e., the capsules) automatic detection, two regions of interest (ROIs) were automatically drawn by a first concentric 30 μm dilation from the external border of the capsule (ROI 1), followed by an additional 100 μm dilation (ROI 2). For both steps, corrections were applied when needed (debris, folds, absence of tissue). To detect the immunostained cells, an optimized colorimetric filter was used, and a detection threshold was empirically determined (Figure 2). Finally, the percentage of stained area was calculated.

2.4 | Methodology validation

Three variables were investigated to validate the methodology: replicability, reproducibility and repeatability. All analyses were performed based on ROI 1.

2.4.1 | Replicability: Inter-observer tissue detection variability

Two independent operators (one naïve and one experienced) analysed a set of sections stained for CD3 and CD68, blindly processing the images (specifically the manual exclusion of non-exploitable areas) but maintaining the same detection threshold.

2.4.2 | Reproducibility: Inter-observer DIA variability

Another set of sections stained for CD68 was analysed by two independent operators (one naïve and one experienced), blindly processing the images and defining independent detection thresholds.

2.4.3 | Repeatability: Immunostaining variability

The same operator analysed different sections of the same biopsy set, independently immunostained (by the same person) for CD68 and CD3 at different time points (4 for CD68; 2 for CD3).

2.4.4 | Comparison with point counting

Images were generated using ImageJ®. Four hundred μm^2 ROIs were drawn at x20 magnification, over selected scanned biopsies, taking the capsular border as one of the limits, and cropped. Using the Grid Tool, one hundred crosses were placed on top of each image and manually counted. A cross was counted as positive if any part of it was in touch with the DAB-stained area. The same images were processed using Visiopharm®, measuring the overall percentage of staining.

2.5 | Statistics

All calculations were computed using IBM SPSS®.

A cubic root transformation was performed to normalize data.

Analyses were done per image, per block (mean value of two images of the same slide) or biopsy (mean values of two or three blocks). For inter-observer correlations, image-to-image comparisons were performed, using intraclass correlation coefficient (ICC). Block-to-block correlations were done using Pearson's. A linear mixed model was used to answer biological questions.

Data are presented as a percentage of IHC positive area in ROI 1 (mean ±standard deviation) unless otherwise stated.

P values <.05 were considered significant.

3 | RESULTS

A summarized workflow of this study is shown in Figure 3.

3.1 | Methodology validation

3.1.1 | Replicability

To assess the inter-observer tissue detection/correction variability, lymphocyte infiltration and macrophage infiltration index were quantified on 31 (CD3) and 46 (CD68) whole slide images.

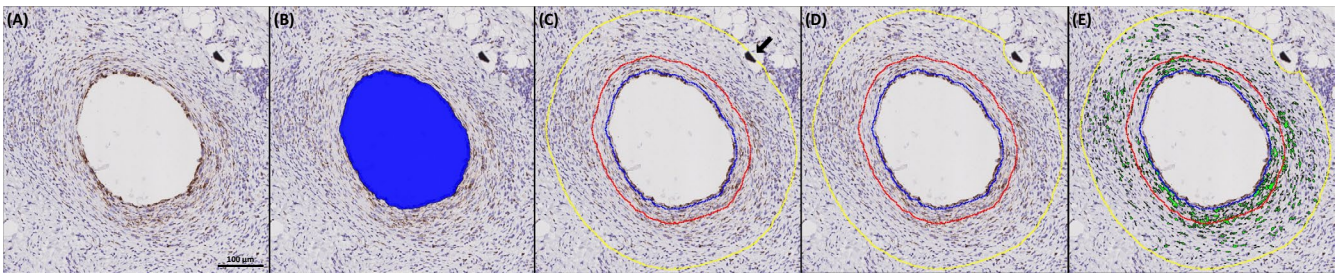

FIGURE 2 Illustration of the semi-automated digital analysis. (A) original image, (B) capsule detection, (C) drawing of ROIs (blue = capsule, red = ROI 1 at 30 μm from capsule border, yellow = ROI 2 at 100 μm from ROI 1 border), (D) manual correction (debris, marked with an arrow) and (E) detection of DAB-stained cells (green)

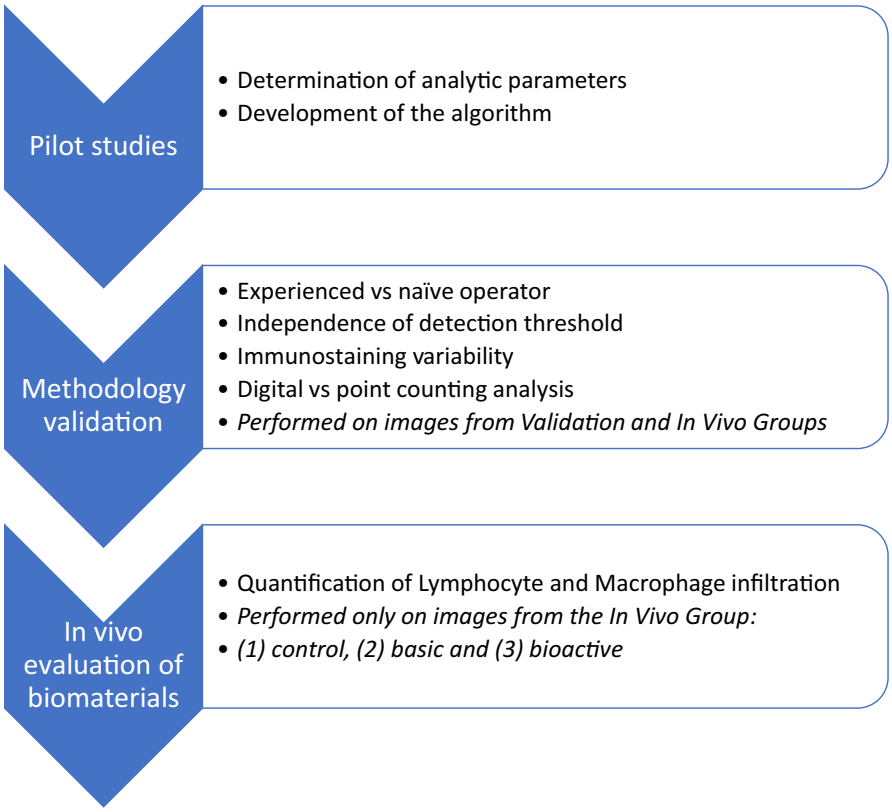

FIGURE 3 Workflow followed for methodology validation and immune infiltrates quantification

Lymphocyte infiltration was 4.42% (±1.89) and 4.70% (±2.07) for operators one and two, respectively. ICC was 0.989 for average measure, with CI95 between 0.946 and 0.996 ($P < .001$).

Macrophage infiltration was 17.07% (±12.94) and 19.00% (±13.94) for operators one and two, respectively. ICC was 0.982 for average measure, with CI95 between 0.941 and 0.993 ($P < .001$).

An experienced operator (the developer of the DIA quantification methodology) and a naïve operator obtained similar, highly correlated results suggesting good automatic capsule detection with minor impact of manual corrections.

3.1.2 | Reproducibility

To evaluate the inter-observer variability in the complete DIA workflow, macrophage infiltration was quantified on whole slide images of 118 sections immunostained for CD68. The infiltration was 10.83% (SD 6.41) and 12.20% (SD 6.40) for operators one and two, respectively. ICC was 0.934 for average measure, with CI95 between 0.852 and 0.965 ($P < .001$). Higher absolute values obtained by operator two (naïve) reflect a less stringent staining detection threshold.

These results show that a DIA workflow requiring minimal corrections produced comparable and highly correlated results, even when independent detection thresholds are used.

3.1.3 | Repeatability

The experimental immunostaining variability was then investigated. Non-consecutive sections (time points 1, 2 and 3) and consecutive sections (time points 3 and 4) of the same biopsies were immunostained, scanned and analysed at the different time points (1 to 4). Values for each time point can be found in the Supporting Information.

For lymphocytes, CD3 IHC was performed only for consecutive sections (time points 3 and 4). Pearson's correlation between blocks was 0.875 (n = 12 per time point, $P < .001$).

For CD68 (macrophages), data from time points correlated as follows: 1 to 2, ICC 0.608, $P < .01$; 1 to 3, ICC 0.476, $P < .01$; 1 to 4, ICC 0.503, $P < .01$; 2 to 3, ICC 0.611, $P < .01$; 2 to 4, ICC 0.394, $P < .05$; and 3 to 4, ICC 0.431, $P < .05$; n = 29 per time point.

Groups stained for CD68 were compared at each time point using a mixed model (see Supporting Information); a statistical difference was evidenced for each paired comparison. These results expose extrinsic variability, resulting in different values at each time point. However, correlations between time points were very strong for CD3 and moderate/strong for CD68. Furthermore, the statistical difference among quantified macrophage infiltration around experimental groups evidences the internal consistency of DIA.

3.1.4 | Point counting

From each section of selected biopsies with IHC for CD3 and CD68, ten images were quantified by point counting (PC) and automated % stained area obtained by DIA. Values of PC were summed per biopsy and compared with DIA values using Pearson's correlation with a listwise approach. Results are summarized in Figure 4.

Although mean values obtained by DIA and PC differ, both methodologies were highly correlated.

3.2 | Evaluation of regions of interest

To explore the influence of the thickness of the ROI, calculations were done on ROI 1, ROI 2 and their sum (ROI 1 + 2).

ROI 1, close to the capsule, represents an area usually infiltrated by immune cells. ROI 2 intended to include tissue of the injection site. The sizes of these ROIs were designed to consider the heterogeneity of infiltrate distribution in the tissue. ROIs correlations are shown in Figure 5.

Moreover, measurements reflected the distribution observed by direct microscopy, where macrophages tend to be found near the capsules (ROI 1) and lymphocytes in the far periphery (ROI 2). Images illustrating this distribution can be found in the Supporting Information.

High correlation among ROIs supports the use of ROI dilatation between 30 and 100 μm from the graft.

3.3 | Biomaterials evaluation

To illustrate the application of this DIA methodology, infiltrates were quantified in the three in vivo Groups previously described: (a) control, (b) basic and (c) bioactive capsules. Comparisons were done using a linear mixed model to exploit the different values obtained for each individual (i.e., each n corresponds to four to six data points). Infiltration was quantified in all ROIs; results for ROIs 1 + 2 are presented in Figure 6.

Taken together, these results show that (a) encapsulated NPI trigger a lymphocytic infiltration; (b) this lymphocytic infiltration is not influenced by the supplementation of hpECM, pMSC and ZW; (c) biomaterials trigger an important macrophage infiltration.

4 | DISCUSSION

The rat subcutaneous tissue has been widely evaluated for experimental transplantation of islets. Porcine islets could be an alternative to humans islets to palliate donors' scarcity.[18]

The immune reaction triggered by grafted encapsulated islets is characterized by immune cell infiltration in the vicinity of the capsule that can lead to graft rejection. To evaluate biocompatibility on experimental biopsies, a DIA protocol was developed, allowing measurement of immune infiltrates. To improve quantification accuracy, each biopsy was cut into three pieces that were processed separately and analysis was performed on entire tissue sections (rather than on selected fields of view). Quantitative DIA in IHC permitted operator independent assessments, using contiguous scales, while relying on objective and standardized criteria for systematic analysis.

DIA has been used for quantification of lymphocytes and macrophages in various contexts.[19,20] In the field of islet transplantation, DIA has been applied on immunofluorescence quantification, although reports lack methodology validation.[9,21] In this study, we present experiments proving an IHC semi-automated quantification methodology that is replicable, reproducible and transposable to two different immunostainings.

The validation procedure permitted exposure of IHC and biological variabilities. When different sections of the same biopsy piece were submitted to the exact same protocol at different time points, the values obtained differed, reflecting irregularities in the immunostaining outcomes, a problem already approached in the literature.[22-24] Another source of irregularities is biological variability, which can be addressed by augmenting the number of analysed slides, which is easily achievable by using DIA. Although extrinsic variability is present, we could evidence correlations among the different time points and the internal coherence of the methodology was proved.

DIA quantification strongly correlated with a widely used method (PC). Values obtained from the latter were higher, as has been described in the literature.[19,25] In addition, the semi-automatization of image analysis allows an important gain in time, which compensates for the costs of DIA software.[26-28]

Using DIA to assess infiltrates has many advantages. Computer-assisted analysis can integrate enormous amounts of data in a comprehensible and efficient fashion. It provides consistent results since objective parameters are clearly defined. In our approach, the user was only asked to identify the non-exploitable tissue, which requires very low expertise and virtually no learning curve.

Nonetheless, some limitations need to be noted. DIA relies on digitalized images of IHC-treated biopsies. Steps occurring before analysis can be influenced by uncontrollable parameters such as human handling, antibodies and solutions' age and quality, and scanning parameters like light intensity. It is therefore important to have quality controls of IHC protocols to ensure repeatable results. In this

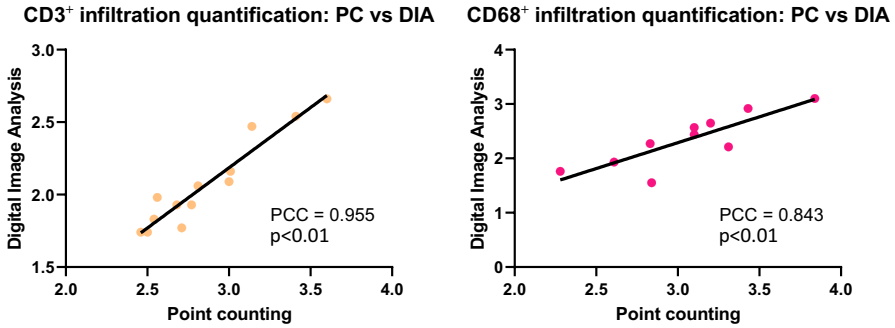

FIGURE 4 Correlations between point counting and digital image analysis with Pearson's correlation coefficient (PCC). CD3 n = 13, CD68 n = 10. Values correspond to transformed data

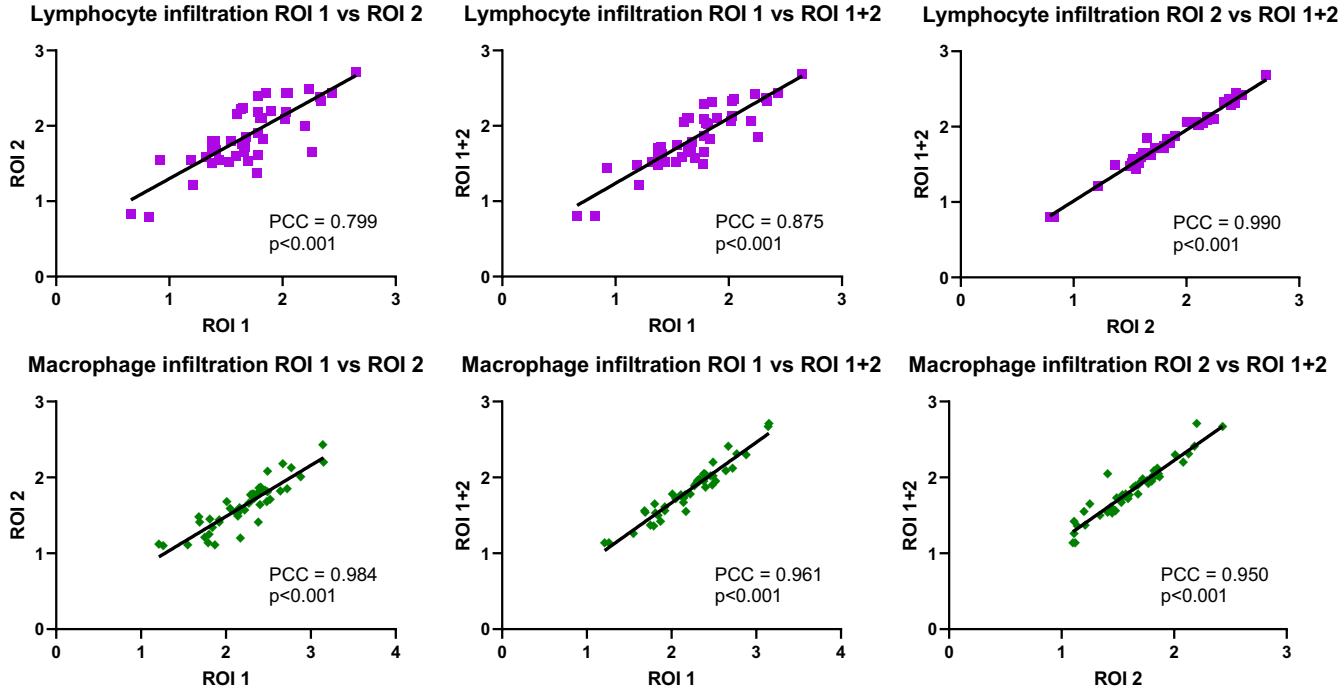

FIGURE 5 Correlations and Pearson's correlation coefficient (PCC) among infiltration measurements for CD3 (lymphocytes, top) and CD68 (macrophages, bottom) in the ROI 1 (proximal ROI), the ROI 2 (distal ROI) and the two ROIs taken together. Values correspond to transformed data

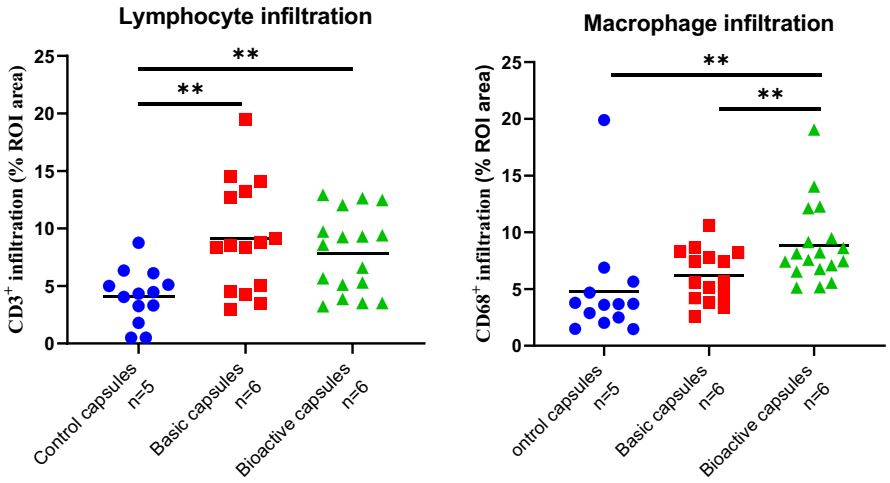

FIGURE 6 Lymphocyte infiltration was higher for both types of capsules containing cells. For macrophages, islets encapsulated in alginate alone triggered less infiltration than those co-encapsulated with biomaterials, with no statistical difference with control capsules. **, $P < .010$. Values correspond to untransformed data

sense, DIA can work retroactively to ensure quality adjustment of IHC protocols.

To show the applicability of DIA, we assessed the biocompatibility of three formulations of capsules grafted subcutaneously in rats. As expected, control (empty) capsules trigger immune infiltration, in line with what has already been described in the literature.[7] The presence of xenogeneic cells inside the basic and bioactive capsules triggers a florid infiltration of lymphocytes, evidencing cellular recognition independent of capsule composition. On the other hand, macrophage infiltration was higher around bioactive capsules, speaking of non-cellular pathways triggered by biomaterials.

Building on our results, more markers could be investigated using the same DIA approach to allow a more extensive evaluation of biocompatibility, such as characterizing subpopulations of the infiltrating cells (eg, macrophage M1/M2 polarization), and evolution of the reaction over time[29,30] or blood vessel distribution.

We offer a new standardized DIA technique to quantify immune infiltration in grafted capsules irrespective of tissue heterogeneity. By this means, we identified the most important source of error as being the immunostaining. We also successfully investigated the biocompatibility of different biomaterials, showing that NPI triggered a milder immune infiltrate when encapsulated in RGD-alginate alone than when co-encapsulated with mesenchymal stem cells, human extracellular matrix and a zwitterionic antifouling coating.

ACKNOWLEDGEMENTS

We would like to thank Pascale Segers, Gwen Beaurin, Daela Xhema and Martial Vergauwen for their cooperation in experiments and manuscript revisions, and Céline Bugli from the SMCS for statistical support.

DATA AVAILABILITY STATEMENT

The data that support the findings of this study are available from the corresponding author upon reasonable request.

ORCID

Matias Ramirez https://orcid.org/0000-0002-7863-5140
Guillaume Courtoy https://orcid.org/0000-0001-9311-2105
Nizar Mourad https://orcid.org/0000-0003-2472-2780

REFERENCES

1. De Mesmaeker I, Robert T, Suenens KG, et al. Increase functional beta-cell mass in subcutaneous alginate capsules with porcine prenatal islet cells but loss with human adult islet cells. *Diabetes*. 2018;67:2640-2649.
2. Scobie L, Galli C, Gianello P, et al. Cellular xenotransplantation of animal cells into people: benefits and risk. *Rev Sci Tech*. 2018;37:113-122.
3. Nishimura M, Iizuka N, Fujita Y, et al. Effects of encapsulated porcine islets on glucose and C-peptide concentrations in diabetic nude mice 6 months after intraperitoneal transplantation. *Xenotransplantation*. 2017;24:e12313.
4. Shimoda M, Matsumoto S. Microencapsulation in clinical islet xenotransplantation. In: Opara E, ed. *Cell Microencapsulation*. New York, NY: Humana Press; 2017:335-345.
5. Mourad NI, Gianello PR. Xenoislets: porcine pancreatic islets for the treatment of type I diabetes. *Curr Opin Organ Transplant*. 2017;22:529-534.
6. Matsumoto S, Abalovich A, Wechsler C, et al. Clinical benefit of islet xenotransplantation for the treatment of type 1 diabetes. *EBioMedicine*. 2016;12:255-262.
7. Veiseh O, Doloff JC, Ma M, et al. Size- and shape-dependent foreign body immune response to materials implanted in rodents and non-human primates. *Nat Mater*. 2015;14:643-651.
8. de Vos P, de Haan BJ, de Haan A, et al. Factors influencing functional survival of microencapsulated islet grafts. *Cell Transplant*. 2004;13:515-524.
9. Stock AA, Manzoli V, De Toni T, et al. Conformal coating of stem cell-derived islets for beta cell replacement in type 1 diabetes. *Stem Cell Rep*. 2020;14:91-104.
10. Veriter S, Gianello P, Igarashi Y, et al. Improvement of subcutaneous bioartificial pancreas vascularization and function by coencapsulation of pig islets and mesenchymal stem cells in primates. *Cell Transplant*. 2014;23:1349-1364.
11. Bouzin C, Saini ML, Khaing KK, et al. Digital pathology: elementary, rapid and reliable automated image analysis. *Histopathology*. 2016;68:888-896.
12. Llacua A, de Haan BJ, Smink SA, de Vos P. Extracellular matrix components supporting human islet function in alginate-based immunoprotective microcapsules for treatment of diabetes. *J Biomed Mater Res A*. 2016;104:1788-1796.
13. Spasojevic M, Paredes-Juarez GA, Vorenkamp J, et al. Reduction of the inflammatory responses against alginate-poly-L-lysine microcapsules by anti-biofouling surfaces of PEG-b-PLL diblock copolymers. *PLoS One*. 2014;9:e109837.
14. Mourad NI, Perota A, Xhema D, et al. Transgenic expression of glucagon-like peptide-1 (GLP-1) and activated muscarinic receptor (M3R) significantly improves pig islet secretory function. *Cell Transplant*. 2017;26:901-911.
15. Dariolli R, Bassaneze V, Nakamuta JS, et al. Porcine adipose tissue-derived mesenchymal stem cells retain their proliferative characteristics, senescence, karyotype and plasticity after long-term cryopreservation. *PLoS One*. 2013;8:e67939.
16. Tamburrini R, Chaimov D, Asthana A, et al. Detergent-free decellularization of the human pancreas for soluble extracellular matrix (ECM) production. *J Vis Exp*. 2020;(163):e61663.
17. Laporte C, Tubbs E, Pierron M, et al. Improved human islets' viability and functionality with mesenchymal stem cells and arg-gly-asp tripeptides supplementation of alginate micro-encapsulated islets in vitro. *Biochem Biophys Res Commun*. 2020;528:650-657.
18. Gianello P. Macroencapsulated pig islets correct induced diabetes in primates up to 6 months. In: Lambris JD, Ekdahl KN, Ricklin D, Nilsson B, eds. *Immune Responses to Biosurfaces*. Cham: Springer International Publishing; 2015:157-170.
19. Nederlof I, De Bortoli D, Bareche Y, et al. Comprehensive evaluation of methods to assess overall and cell-specific immune infiltrates in breast cancer. *Breast Cancer Res*. 2019;21:151.
20. Peng JZ, Gutstein DE, Beck L, et al. Quantifying monocyte infiltration in response to intradermal tetanus toxoid injection. *Biomark Med*. 2012;6:541-551.
21. Fransson M, Brannstrom J, Duprez I, et al. Mesenchymal stromal cells support endothelial cell interactions in an intramuscular islet transplantation model. *Regen Med Res*. 2015;3:1.
22. Baker M. Reproducibility crisis: blame it on the antibodies. *Nature*. 2015;521:274-276.
23. Hamilton PW, Bankhead P, Wang Y, et al. Digital pathology and image analysis in tissue biomarker research. *Methods*. 2014;70:59-73.
24. Walker RA. Immunohistochemical markers as predictive tools for breast cancer. *J Clin Pathol*. 2008;61:689-696.
25. Buisseret L, Garaud S, de Wind A, et al. Tumor-infiltrating lymphocyte composition, organization and PD-1/ PD-L1 expression are linked in breast cancer. *Oncoimmunology*. 2017;6:e1257452.
26. Jahn SW, Plass M, Moinfar F. Digital pathology: advantages, limitations and emerging perspectives. *J Clin Med*. 2020;9:3697.
27. Maguire AS, Woodie LN, Judd RL, et al. Whole-slide image analysis outperforms micrograph acquisition for adipocyte size quantification. *Adipocyte*. 2020;9:567-575.
28. Miksch RC, Hao J, Schoenberg MB, et al. Development of a reliable and accurate algorithm to quantify the tumor immune stroma (QTiS) across tumor types. *Oncotarget*. 2017;8:114935-114944.
29. Badylak SF, Valentin JE, Ravindra AK, et al. Macrophage phenotype as a determinant of biologic scaffold remodeling. *Tissue Eng Part A*. 2008;14:1835-1842.
30. Ibarra V, Appel AA, Anastasio MA, et al. This paper is a winner in the Undergraduate category for the SFB awards: Evaluation of the tissue response to alginate encapsulated islets in an omentum pouch model. *J Biomed Mater Res A*. 2016;104:1581-1590.

SUPPORTING INFORMATION

Additional supporting information may be found online in the Supporting Information section.

How to cite this article: Ramirez M, Courtoy G, Kharrat O, et al. Semi-automated digital quantification of cellular infiltrates for in vivo evaluation of transplanted islets of Langerhans encapsulated with bioactive materials. *Xenotransplantation*. 2021;28:e1–7. https://doi.org/10.1111/xen.12704